Smart Structures and Systems, *Vol. 27, No. 2 (2021) 267-284*
DOI: https://doi.org/10.12989/sss.2021.27.2.267

Response based track profile estimation using observable train models with numerical and experimental validations

Jothi Saravanan Thiyagarajan [1,2a], Di Su[*2], Hirofumi Tanaka [3b], Boyu Zhao [4c] and Tomonori Nagayama [2d]

[1] *School of Infrastructure, Indian Institute of Technology Bhubaneswar, Odisha 752-050, India*
[2] *Department of Civil Engineering, The University of Tokyo, Tokyo 113-8656, Japan*
[3] *Track Technology Division, Railway Technical Research Institute, Tokyo 185-8540, Japan*
[4] *Takasaki Railway Maintenance Center, East Japan Railway Company, Gunma 370-0841, Japan*

(*Received July 3, 2020, Revised September 9, 2020, Accepted October 23, 2020*)

Abstract. Condition monitoring of railway tracks is essential in guaranteeing the running safety of railways. Track profiles are the primary source of external excitation for a train system. While Track Recording Vehicle is often utilized for maintenance purposes, this particular vehicle is expensive and difficult to use for small railway operators. Therefore, track profile estimation through in-service vehicle response measurements, which potentially provides efficient and frequent measurement, has been studied. However, the quantitative evaluation of the vertical and lateral track profile irregularities is still challenging as the inverse analysis solutions are sometimes inaccurate and even unstable. In this paper, numerical analyses are first carried out to evaluate track profiles from acceleration and angular velocity responses measured on a train car body. For the inverse analysis, an Augmented State Kalman Filter is utilized to solve the problem using 4 degrees of freedom observable train models. The sensor installation locations are investigated through observability rank condition analysis with different measurement layout. Secondly, a field experiment is carried out in a local Japanese in-service railway network to estimate track profile from car body motions. Smartphones are utilized for the field test measurements as prevalent sensing devices. The effectiveness of the proposed approach is demonstrated with the observable train model. Numerical analyses and field experiments clarify the proposed track profile estimation's capability using only one on-board sensing device.

Keywords: railway track profile; inverse analysis; observability; Augmented State Kalman Filter; smartphone measurement; train model

1. Introduction

A train vehicle running on the railway track is a complex dynamic system with many components. Track profile, which directly influences the ride quality and safety, need to be estimated. Track irregularities, otherwise known as profile characteristics, have been troubling railway engineers (Bruni *et al*. 2007). The necessary inspections need to be performed for determining the track condition. Conventionally, track profile measurement is done using the Track Recording Vehicle (TRV). While accurate track profile is obtained, small railway operators may not afford the special vehicle. Even for large railway operators, frequent quantitative evaluation of the railway track with short intervals is not feasible. TRVs typically pass through only once every few weeks or few months. Track profile evaluation using sensors on in-service vehicles potentially overcomes these issues (Barke and Chiu 2005, Weston *et al*. 2015). Sensors placed on an in-service train vehicle can collect a large amount of data as the vehicle can cover the same track several times every day (Ward *et al*. 2011). A few robust sensors such as accelerometers and rate gyroscopes are mounted on the bogie and axle boxes of an in-service train vehicle for monitoring ride quality (Chiacchiari and Loprencipe 2015). A field test was carried out in a train car of a public transportation company in Milan, Italy, using accelerometers on operating bogies. A proper numerical model was required to handle highly complex train dynamics besides the wavelet-based approach for signal processing (Bocciolone *et al*. 2007). Lately, vertical acceleration measurements at axles of regular service trains in Italian transportation have been utilized for monitoring track profile (Real *et al*. 2011). In pioneering work carried out by Japanese researchers, axle box accelerometers to observe rail corrugation from in-service vehicles have been investigated (Sunaga *et al*. 1997). Later, Naganuma and Sato (2000) introduced an economical way to track maintenance planning with the use of real-time digital data processing from the inertial measurement unit, which eliminates the waveform distortion. The track condition evaluation considering vehicle dynamics and human sensibility was achieved using a monitoring device

*Corresponding author, Ph.D., Associate Professor,
E-mail: su@bridge.t.u-tokyo.ac.jp
[a] E-mail: tjs.saravanan@gmail.com
[b] E-mail: tanaka.hirofumi.96@rtri.or.jp
[c] E-mail: h-chiyou@jreast.co.jp
[d] E-mail: nagayama@bridge.t.u-tokyo.ac.jp

ISSN: 1738-1584 (Print), 1738-1991 (Online)

installed at the axle box. Weston *et al*. (2007a, b) discussed using sensors mounted on the bogie of an in-service vehicle to monitor vertical track and lateral track irregularities, respectively. Recently, an Irish Rail intercity train was instrumented for longitudinal track profile estimation, using bogie vertical inertial measurements, and cross-entropy optimization technique was utilized for further data processing (Obrien *et al*. 2017, 2018). However, these methods using sensors on bogies or axles are often not implemented for the service train model due to practical problems in mounting and wiring sensors; safe railway operation concerns and installation costs are among the reasons to avoid such sensors.

Sensors on vehicle bodies can be easily installed and have been studied. Kojima *et al*. (2006) introduced the probe vehicles for rail maintenance, and the vehicles contributed to improving the safety of the transport systems. The proposal introduced a wavelet-based multi-resolution analysis method for detecting faults by decomposing the acceleration response measured on the train car body. Ishii *et al*. (2006) developed a low-cost Train Intelligent Monitoring System for monitoring railway track irregularities of local railways; the system could identify irregularities and their positions using an accelerometer and a GPS mounted on the train car body. Only the abnormal acceleration data can be detected for the change of track status by comparing daily measurement.

In recent times, the inverse analysis technique based on a Kalman filter is utilized for estimating track irregularities. The main drawback of using the Kalman filter technique tends to attain an unstable solution. This is due to the inappropriate train model utilized for the inverse analysis. In recent times, both Kobayashi *et al*. (2014) and Tsunashima *et al*. (2014) researched track profile estimation of a Shinkansen track in Japan from car body acceleration using the inverse analysis technique based on a conventional augmented Kalman filter. The same research group carried out track profile estimation for conventional railway track using car-body acceleration only (Odashima *et al*. 2017). The augmented Kalman filter, whose observation variable was car body vertical acceleration, is incidentally unobservable. Henceforth, the inverse analysis cannot be stably solved for further evaluation without addressing the observability issue (Lourens *et al*. 2012, Zhao *et al*. 2019, Xue *et al*. 2020).

The following are identified as the drawbacks of previous research: (a) mounting sensors on bogie and axles have practical difficulties; (b) inverse analysis has observability issues making it difficult to obtain stable results. A simple, robust, and cost-effective method for track profile estimation using multiple outputs measured by a sensor installed on in-service train vehicle is proposed in this study to address these issues. The idea for the railway track profile estimation is inspired by the previous work (Zhao *et al*. 2019), which deals with road profile estimation. For inverse analysis, an augmented Kalman filter technique can be utilized for estimating the unknown inputs. The track profile is included in the form of augmented state variables and estimated through Kalman filtering. However, the issue of observability needs to be solved. Therefore, the Observability Rank Condition (ORC) of an extended Augmented State Kalman Filter (ASKF) is discussed. The simple acceleration and angular velocity measurements are obtained by utilizing a limited number of sensors attached to the train car body. The observable train models capable of representing the rigid body motion are employed to evaluate both vertical and lateral track profiles. Firstly, numerical analyses are carried out using 4 degrees of freedom (DOF) train models; the proposed ASKF technique, which satisfies the observability condition, performs better than the conventional method. Finally, to validate the estimation algorithm, a field test is conducted on a Japanese local railway line using smartphones installed on the train car body. Thus, this research clarifies the capability of the proposed track profile estimation using only one on-board sensing device through numerical analyses and field experiments.

2. Train vehicle model

For the inverse analysis to obtain the track profile, a 4-DOF half-car train model with averaged track profile is utilized. While a train vehicle has four axles, the front two and rear two axles are on the front bogie and rear bogie, respectively. According to the authors' previous research, the complicated vehicle model has difficulty obtaining stable and accurate inverse analysis results (Zhao *et al*. 2019, Xue *et al*. 2020), which will be explained in the following sections. The fundamental reason is that the minimal measurement sets are not enough to address the observability issue. Therefore, in this study, a 4-DOF model is considered with the axles' average motions on each bogie as the input to the train system. The bogie's pitching and yawing motion are not considered in the train model by taking only the averaged profile. On comparing with the direct profile estimation from each wheel, the averaged profile does not contain a frequency component corresponding to the wavelength of twice of the wheelbase of the bogie (around 4.5 m) (JSME 1996, JRCEA 2002), which generally falls under the category of the short-wavelength track irregularities (not of our range of interest). Moreover, in the experimental conditions, it is good enough for the railway operators to know the average of track irregularity as it is managed using 10 m-chord versines whose wavelength band of about 10 m for the running safety.

The following set of measurements is necessary for estimating track profile, i.e., car body vertical acceleration and pitching angular velocity for a vertical profile, car body lateral acceleration, and yawing angular velocity for a lateral profile. The 4-DOF train model to estimate vertical and lateral profiles are presented in Figs. 1(a) and (b), respectively. In Fig. 1(a), z_c and θ_c are the car body vertical translational displacement and pitch angle, z_{t1} and z_{t2} are front and rear bogie vertical displacement. The inputs, r_{1a}, r_{1b}, r_{2a} and r_{2b}, denote the vertical track displacement. In Fig. 1(b), y_c and φ_c are the car body lateral translational displacement and yaw angle, y_{t1} and y_{t2} are front and rear bogie lateral displacement. The

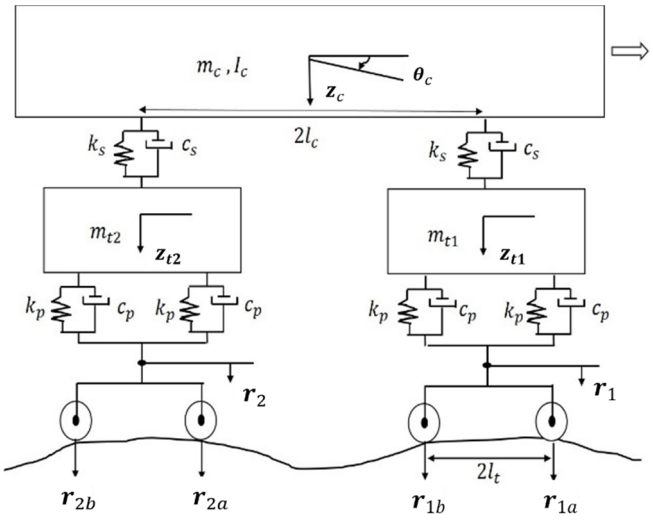

(a) A vertical profile estimation model

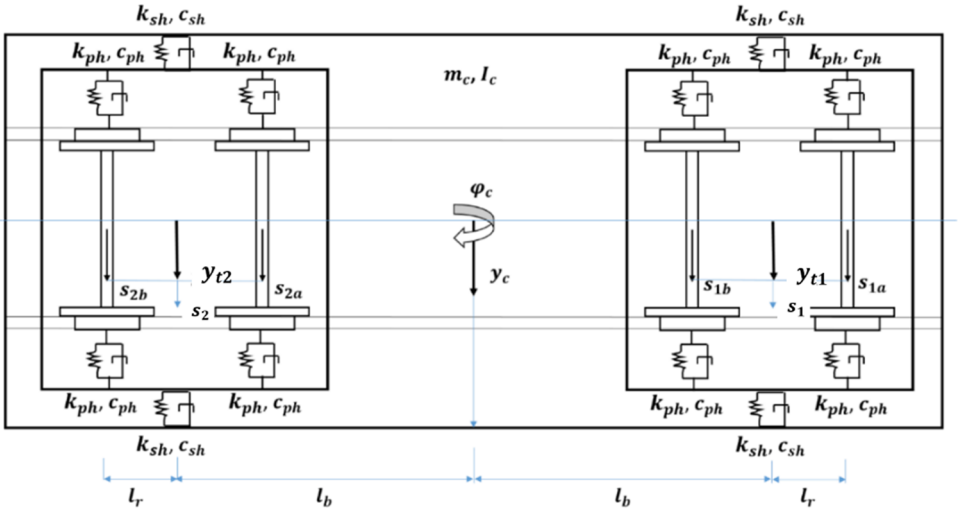

(b) A lateral profile estimation model

Fig. 1 4-DOF train model with averaged track profile

inputs, s_{1a}, s_{1b}, s_{2a} and s_{2b}, denote the lateral track displacement.

Using Lagrange equations, the dynamic equations of motion for the 4-DOF model are derived for the vertical (denoted with subscript 'v') and lateral (denoted with subscript 'l') directions, respectively, as follows.

$$M_v\ddot{z}(t) + C_v\dot{z}(t) + K_v z(t) = Dr(t) + E\dot{r}(t) \quad (1)$$

$$M_l\ddot{y}(t) + C_l\dot{y}(t) + K_l y(t) = Fs(t) + G\dot{s}(t) \quad (2)$$

where M_v, M_l are system mass matrices; C_v, C_l are damping matrices; K_v, K_l are stiffness matrices; $z(t)$ and $y(t)$ are displacement vectors; $r(t)$ and $s(t)$ represent the track profiles as a function of time. D, E, F, and G are the matrices prescribing the force, as explained in Appendix A and B. Because the train models do not include the bogie's pitching and yawing motion, an external force vector containing eight elements (track profile at four wheels and their respective first derivative) cannot be estimated only from the car body response measurement. Thus, an averaged track profile between each bogie's front and rear axle is considered, transmitted to the train car body. The front and rear average profiles are given as

$$r_1 = \frac{r_{1a} + r_{1b}}{2}; \quad r_2 = \frac{r_{2a} + r_{2b}}{2}; \quad r^T(t) = [r_1, r_2] \quad (3)$$

$$s_1 = \frac{s_{1a} + s_{1b}}{2}; \quad s_2 = \frac{s_{2a} + s_{2b}}{2}; \quad s^T(t) = [s_1, s_2] \quad (4)$$

Consider state vectors containing the average profiles of $r(t)$ and $s(t)$. The state vectors for the vertical and lateral direction equations are as follows.

$$x_v^a = [z_c\ \theta_c\ z_{t1}\ z_{t2}\ \dot{z}_c\ \dot{\theta}_c\ \dot{z}_{t1}\ \dot{z}_{t2}\ r_1\ r_2\ \dot{r}_1\ \dot{r}_2]^T \quad (5)$$

$$x_l^a = [y_c\ \varphi_c\ y_{t1}\ y_{t2}\ \dot{y}_c\ \dot{\varphi}_c\ \dot{y}_{t1}\ \dot{y}_{t2}\ s_1\ s_2\ \dot{s}_1\ \dot{s}_2]^T \quad (6)$$

The following sections are explained mainly for the vertical case, while the contents of these sections are directly applicable to the lateral case by changing the

governing equation and the state vector to those corresponding to the lateral direction, respectively.

3. Track profile estimation algorithm

3.1 Augmented state-space model

The proposed inverse analysis method for track profile estimation in this study comprises a standard linear Kalman filter **tec1**

hnique with an augmented state-space representation where the dynamic input forces are augmented to the state vector (Kalman 1963). The profile estimation has been derived using the augmented state-space models. Consider a linear, discrete-time dynamical system in state-space with a state vector, x_k. The subscript *k* represents discrete time.

$$x_{k+1} = Ax_k + Bu_k + w_k \tag{7}$$

$$f_k = Hx_k + Gu_k + v_k \tag{8}$$

where *A* and *B* represent transition matrix and input matrix, respectively; *H* is the measurement matrix; *G* is the direct transmission matrix. u_k denotes the dynamic input excitation vector; w_k denotes stochastic process noise vector, where the noise is additive, white, and Gaussian with zero mean; f_k is the measurement vector; v_k is the measurement noise, where the noise is additive, white, and Gaussian with zero mean and uncorrelated with the process noise. By redefining the state vector by adding the unknown input vector, an augmented state equation is obtained along with a noise vector (ε_k)

$$x_k^a = [x_k\ u_k\ ] \tag{9}$$

$$x_{k+1}^a = [A\ B\ 0\ I\ ]x_k^a + \{w_k\ \eta_k\ \} = A_a x_k^a + \varepsilon_k \tag{10}$$

where A_a is the transition matrix (shown in Appendix A); η_k is a component of the stochastic process (Fauriat *et al*. 2016), which can be presented as

$$u_{k+1} = u_k + \eta_k \tag{11}$$

The measurement equation of the augmented state-space model has the following form

$$f_k = H_a x_k^a + v_k \tag{12}$$

where H_a is the new measurement matrix constructed from H and G, represented as

$$H_a = [H\ \ G] \tag{13}$$

Hence, the formulation for augmented state-space model are given in Eqs. (10) and (12) respectively.

3.2 ASKF for input-state estimation

The current method for recursive joint state-input estimation is the ASKF inverse analysis technique, which is considered an optimal estimator in a minimum-variance unbiased sense, i.e., to infer parameters from indirect and uncertain measurements ultimately. The objective mentioned above to extract input force from dynamic measurements can be achieved by implementing the ASKF technique, which conventionally follows a recursive prediction-correction pattern. Let $\hat{x}_k^a$ be the posterior state estimate of x_k^a. Without observed data at time k = 0, the initial state estimate is given as, $\hat{x}_0^a$ and it is assumed to be a random variable. A posterior state estimate is derived by combining the prior estimate $\hat{x}_k^{a-}$ (Prediction step) and the weighted difference between actual measurement and a measurement prediction $H_a\hat{x}_k^{a-}$ (Update step) as illustrated below.

$$\hat{x}_k^a = \hat{x}_k^{a-} + L(f_k - H_a\hat{x}_k^{a-}) \tag{14}$$

The difference $(f_k - H_a\hat{x}_k^{a-})$ is known as the measurement residual, which reveals the inconsistency between the predicted and the actual measurement. The matrix *L* is called the Kalman gain, an essential factor that minimizes the posterior error covariance. Henceforth, the error covariance matrix P_k will have the following form with the assumption that P_0 and $\hat{x}_0^a$ are known.

$$P_k = E[(x_k^a - \hat{x}_k^a)(x_k^a - \hat{x}_k^a)^T] \tag{15}$$

The covariance matrices of $\{w_k\}, \{\eta_k\}\ and\ \{v_k\}$ are defined as

$$E[w_k w_k^T] = Q \qquad E[\eta_k \eta_k^T] = S \qquad E[v_k v_k^T] = R \tag{16}$$

The process noise covariance matrix *Q* is based on the system's model error, and the observation noise covariance matrix *R* depends on the accuracy of sensors and modeling error in the observation equation. The ASKF formulation for the discrete-time state-space model of a physical system is presented in terms of time update [Eqs. (17)-(18)] and measurement update [Eqs. (19)-(21)].

$$\hat{x}_{k+1|k}^a = A_a\hat{x}_{k|k}^a \tag{17}$$

$$P_{k+1|k} = A_a P_{k|k} {A_a}^T + Q_a \tag{18}$$

$$L_{k+1} = P_{k+1|k}H_a^T(H_a P_{k+1|k}H_a^T + R_{k+1})^{-1} \tag{19}$$

$$\hat{x}_{k+1|k+1}^a = \hat{x}_{k+1|k}^a + L_{k+1}(f_{k+1} - H_a\hat{x}_{k+1|k}^a) \tag{20}$$

$$P_{k+1|k+1} = P_{k+1|k} - L_{k+1}H_a P_{k+1|k} \tag{21}$$

Considering the expressions mentioned above, if the observation noise covariance matrix *R* approaches zero, the Kalman gain *L* affects the residual severely, i.e., the actual measurement is trusted more. Instead, if the prior estimate error covariance matrix approaches zero, then the residual gain matrix is less, else the predicted measurement is trusted. Though significant modeling error can be compensated by increasing the system noise covariance, the track profile estimation accuracy may be sacrificed. In combination with the augmented noise vector ε_k of Eq.

(10), the augmented covariance matrix Q_a is given as

$$Q_a = \begin{bmatrix} Q & 0 \\ 0 & S \end{bmatrix} \tag{22}$$

3.3 Observability analysis

The profile estimation capability through the linear Kalman filter technique is first investigated through an ORC analysis. A system is observable if the present state can be obtained finite time using only the outputs (Hermann and Krener 1977). If a system is not observable, some of its states; current values cannot be determined through output measurements. A linear state-space model with N state variables is observable if and only if, the rank of the observability matrix $[O]$ is equal to N

$$O = \begin{bmatrix} H_a \\ H_a A_a \\ H_a A_a^2 \\ \vdots \\ H_a A_a^{N-1} \end{bmatrix} \tag{23}$$

where, A_a is the transition matrix and H_a is the measurement matrix. Even when the system is unobservable, some state variables can still be estimated. A subset of the unobservable state vector is considered to have observable state variables (Chatzis *et al*. 2015). The observability algorithm for the linear system can examine the ORC of the state variables by excluding the i^{th} column of the matrix $[O]$ and examining the resultant matrix's rank. If the rank is less than the original matrix $[O]$, the i^{th} state is observable; otherwise, it is not. Hence, the observable state variables can be separated from the unobservable variables.

3.4 Proposed approach for track profile estimation

The augmented state-space model and Kalman filtering techniques are employed for the track estimation problem. The ORC analysis of the time-invariant 4-DOF train model is carried out to obtain the appropriate sensor placement strategy (Saravanan *et al*. 2016). All possible combinations of measurement at car body with an accelerometer and a gyro and bogies with accelerometers are analyzed in terms of ORC, and the observability of the state variables, including the profiles and their derivatives, are examined. The ORC analysis results for the vertical train model are shown in Table 1 as a typical case. None of the profile state variables is observable. To overcome this issue, a new approach is proposed as an extension of the augmented state-space model. It is based on the idea that the second derivative of the profile can be observable only from acceleration measurement while the profile and its first derivative are not.

Table 1 ORC analysis for 4-DOF train model using the proposed approach

Measurements	Observable states	
	Conventional	Proposed approach
$\ddot{z}_c$	Nil	Nil
$\dot{\theta}_c$	$\dot{\theta}_c$	$\dot{\theta}_c$
$\ddot{z}_c\ \dot{\theta}_c$	$\dot{\theta}_c$	$\dot{\theta}_c\ \ddot{r}_1\ \ddot{r}_2$
$\ddot{z}_{t1}$	Nil	$\ddot{r}_1$
$\ddot{z}_{t2}$	Nil	$\ddot{r}_2$
$\ddot{z}_c\ \dot{\theta}_c\ \ddot{z}_{t1}\ \ddot{z}_{t2}$	$\dot{\theta}_c$	$\dot{\theta}_c\ \ddot{r}_1\ \ddot{r}_2$

In the proposed approach, the state variables are augmented with the second derivative of the profile and estimate the second derivative. The profile is estimated as the double integration of the augmented state variable. A high pass filter removes the double integration error. The new state vector for the vertical displacement train model is expressed as follows

$$\tilde{x}_v^a = [z_c\ \theta_c\ z_{t1}\ z_{t2}\ \dot{z}_c\ \dot{\theta}_c\ \dot{z}_{t1}\ \dot{z}_{t2}\ r_1\ r_2\ \dot{r}_1\ \dot{r}_2\ \ddot{r}_1\ \ddot{r}_2]^T \tag{24}$$

The new augmented state vector's transition matrix as per Eq. (24) is expressed in Appendix C, corresponding to the proposed approach. As discussed, the conventional ASKF method, by using x_v^a as the state vector, have determined likely to have numerical instabilities due to the augmented state-space model's problems. To overcome this issue of un-observability, the proposed state vector in Eq. (24) satisfies the observability condition, and this process makes the second derivative of the profile as an observable state even though the profile is not observable. The ORC analysis results of the proposed approach are tabulated in Table 1. Note that only limited combinations are listed in the table. While the inclusion of integrated quantities in the observation to satisfy the observability takes advantage of the inclusion to achieve the observability by only using a single sensor unit.

The measurement of only the body acceleration, which is often common practice for track irregularities monitoring using the in-service train, does not make the profiles or the derivatives observable. Only angular velocity on the car body does not make the profiles or the derivatives observable. On the other hand, the combination of acceleration and angular velocity measurements on the car body results in observable profile derivatives. Acceleration measurement on a bogie also makes the second derivative of the profile under the bogie observable. Since this research investigates track irregularities monitoring assuming easy sensor installation only in the car body, acceleration and angular velocity are measured on the car body. The profiles are obtained by the double integration of the high pass-filtered second derivatives. The cut-off frequency of the high-pass filter is set considering track profile wavelength range of interest. Note that even when acceleration and angular velocity at all of the 4-DOF are measured, the profiles are not observable; only the second derivatives are observable. The ORC analysis results and inferences are the same for the lateral profile estimation model.

4. Numerical validation

The Kalman filter's performance is influenced by filter

parameters such as process and measurement noise covariance matrices. Incorrect parameters can result in divergence, instability, or convergence toward faulty values. The covariance matrices Q, S, and R are usually diagonal matrices and need to be appropriately set. The measurement noise is primarily the sensor noise and the noise from vehicle engine vibration. The noise levels are experimentally determined through the smartphone static measurement test and the vibration measurement on a stationary vehicle while its engine is idling. The first eight diagonal components of Q are tuned, while the last four components corresponding to the track profiles and their derivatives are kept constant. As for the process noise, the covariance is set by reference to the rate of state variables' change in the same manner as in other Kalman filter applications. The validity of these methods with the tuned covariance matrices is examined through numerical simulation herein.

4.1 Simulated railway track irregularity

Track irregularity (profile characteristics) can be given as random functions regarding the longitudinal coordinate axis 'x'. Numerous measurements have shown that the track irregularities can be described by a one-sided Power Spectral Density (PSD) function of the track geometry (Fries and Coffey 1990). PSD functions utilized in this study are expressed in Eqs. (25) and (26) for elevation, alignment, and cross irregularities.

$$S_{v,a}(\Omega) = \frac{A_v \Omega_c^2}{(\Omega^2 + \Omega_r^2)(\Omega^2 + \Omega_c^2)} \tag{25}$$

$$S_c(\Omega) = \frac{A_v \Omega_c^2 \Omega^2 / l_a^2}{(\Omega^2 + \Omega_r^2)(\Omega^2 + \Omega_c^2)(\Omega^2 + \Omega_s^2)} \tag{26}$$

where $S_{v,a}$ is PSD function for the elevation and alignment irregularity; S_c is PSD function for the cross-level irregularity; A_v is surface roughness constant; $\Omega = \frac{1}{L_r}$ represents the spatial frequency (rad/m); L_r is the length of the irregularity (m); Ω_c, Ω_r and Ω_s represent the spatial frequency corresponding to cross-level, elevation, and gauge irregularities, respectively. The Federal Railroad Administration (FRA) classifies the tracks as Classes 4, 5, and 6, with Class 6 representing the best and Class 4 the worst. On comparing three cases, Class 4 represents the worst condition of the track profile, which is more significant for running safety. Thus, it is worth discussing the proposed estimation algorithm results related to Class 4 in this research. Table 2 illustrates the values of FRA's coefficients for the Class 4 track (Fries and Coffey 1990, Su *et al*. 2010). The track irregularity represented in the spatial frequency domain is converted to profiles in the spatial domain and then to those in the temporal domain, assuming a train drive speed. Simulated rail irregularities in the spatial domain are produced by the spectral representation method (Claus and Schiehlen 1998).The vertical (r_{vl}) and alignment (r_{hl}) profile irregularities for left rail are calculated as follows

Table 2 Track PSD model parameter (Fries and Coffey 1990)

Quality (FRA)	A_v (m)	Ω_s (rad/m)	Ω_r (rad/m)	Ω_c (rad/m)
Very poor (Class 4)	2.39×10^{-5}	1.130	2.06×10^{-2}	0.825

$$r_{vl}(x) = r_v(x) + \frac{r_c(x)}{2} \tag{27}$$

$$r_{hl}(x) = r_h(x) \tag{26}$$

where r_v, r_c, and r_h are elevation, cross-level, and alignment of a twin rail system. Similarly, profile irregularities for the right rail can be calculated. The track profiles used for simulation are plotted in Fig. 2. Both left and right rails are assumed to have identical track irregularities corresponding to vertical and lateral track profiles. The corresponding wavelength is 0.5 m to 300 m. As per European standards (BS 2003), the wavelength considered for track irregularities ranges from 3 m to 200 m (even for high-speed railways); for Japanese conventional lines (Yoshimura 1995), the wavelength is 6 m to 60 m, which covers short to long-wavelength track irregularities.

4.2 Quantification through various metrics

To validate the estimation algorithm, the following metrics have been used to quantify the estimation error.

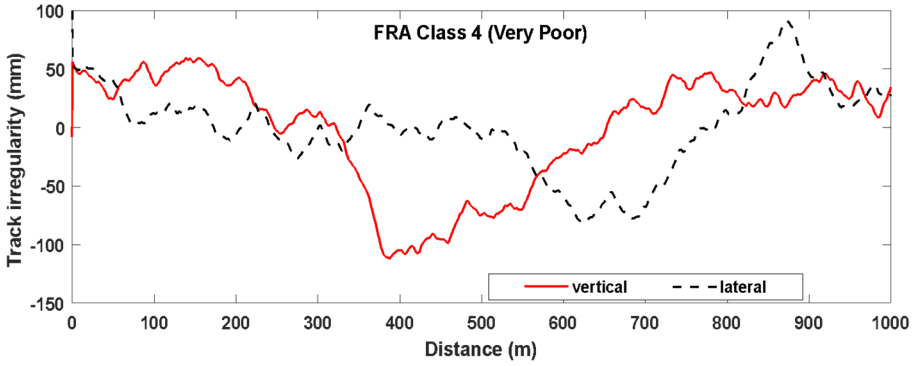

Fig. 2 Rail Track profile: generated from FRA Class 4

4.2.1 Root Mean Square Error/ Deviation

Root Mean Square Error (RMSE) is a dimensional error estimation value, while Root Mean Square Deviation (RMSD) is a normalized value (Giurgiutiu and Rogers 1998).

$$RMSE\ (mm) = \sqrt{\frac{\sum_{i=1}^{n}(X_i - Y_i)^2}{n}} \tag{29}$$

$$RMSD\ (\%) = \sqrt{\frac{\sum_{i=1}^{n}(X_i - Y_i)^2}{\sum_{i=1}^{n}(X_i)^2}}\, x\ 100 \tag{30}$$

where X_i and Y_i are the i^{th} values of reference series and compared series respectively, and n is the number of data samples.

4.2.2 Correlation coefficient

Correlation identifies similarity and dependency among two waveforms. An exact resemblance indicates that the Correlation Coefficient (CC) is unity (Park and Inman 2007).

$$CC = \frac{1}{n-1}\sum_{i=1}^{n}\left(\frac{X_i - \underline{X}}{s_X}\right)\left(\frac{Y_i - \underline{Y}}{s_Y}\right) \tag{31}$$

$$\underline{X} = \frac{1}{n}\sum_{i=1}^{n} X_i\,; \quad s_X = \sqrt{\frac{1}{n-1}\sum_{i=1}^{n}(X_i - \underline{X})^2} \tag{32}$$

where $\underline{X}$ and s_X are the sample mean and sample standard deviation, respectively, and n is the number of data samples.

4.3 Investigation on track profile estimation

For track profile estimation, the ASKF method is numerically investigated. While the 4-DOF model in Fig. 1 is employed in the ASKF, a 6-DOF model, which also has a rolling motion of each bogie (yawing motion for lateral case), is utilized the forward simulation to calculate train responses. The responses are obtained assuming accelerometers and rate gyro sensors mounted on the car body floor just above the front bogie mass. The 6-DOF train model's measurement responses are given as the input responses for the 4-DOF model in the inverse analysis. The 6-DOF model is not directly used for the inverse analysis as the model is not observable for only car body floor measurements. The reference vehicle parameters representing local railway train are obtained from JSME (1996) and JRCEA (2002), as shown in Table 3. These vehicle parameters correspond to a conventional express train type vehicle. The vehicle retains a constant velocity of 90 km/h, which is common for express trains in Japan. The simulation distance is 1000 m, and the sampling frequency is 100 Hz. Vehicle model errors and measurement noises are taken into account.

The response is simulated by adding noise components to the measured vehicle responses as

$$M_{noise} = M + \in \gamma_{noise}\sigma(M) \tag{33}$$

Table 3 Train vehicle model parameters (JSME 1996, JRCEA 2002)

Parameter	Value
Car body mass (m_c)	11571.5 kg
Front bogie mass (m_{t1})	2042.5 kg
Rear bogie mass (m_{t2})	2042.5 kg
Car body mass moment of inertia (I_c)	416574 kg m^2
Front bogie mass moment of inertia (I_{t1})	1211 kg m^2
Rear bogie mass moment of inertia (I_{t2})	1211 kg m^2
Primary vertical suspension stiffness (k_p)	1150 kN/m
Secondary vertical suspension stiffness (k_s)	290 kN/m
Primary vertical suspension damping (c_p)	115 kN s/m
Secondary vertical suspension damping (c_s)	29 kN s/m
Primary horizontal suspension stiffness (k_{ph})	3840 kN/m
Secondary horizontal suspension stiffness (k_{sh})	176 kN/m
Primary horizontal suspension damping (c_{ph})	384 kN s/m
Secondary horizontal suspension damping (c_{sh})	17.6 kN s/m
Half of the car body base (l_c)	7.2 m
Half of the bogie-wheel base (l_t)	1.125 m

where $\in$ is the percentage noise level, γ_{noise} is a noise with a standard normal distribution, $\sigma(M)$ is the standard deviation of the measured response. Noise is added to estimated responses based on the features of practical sensors. The bandpass filter with the cut-off frequency of 0.0166-0.166 cycle/m is considered in this simulation to evaluate short to long-wavelength (λ) irregularities ranging between 6 m and 60 m (Tanaka *et al*. 2017). A high-pass filter with a cut-off frequency of 0.15 Hz is applied to the second derivative of the profile to remove the low-frequency integration error. In this research, the longest wavelength considered is 60 m. The high-pass filter is applied in the time domain. While the cut-off frequency is kept constant in the temporal domain, the spatial domain frequency depends on the drive speed. For the temporal cut-off frequency of 0.15 Hz, the corresponding spatial frequency is less than the lower cut-off frequency of the bandpass filter ($1/\lambda$ < 0.0166 cycle/m) as long as the train speed is above 35 km/h. Lower drive speeds result in higher cut-off spatial frequency and underestimate or ignore low spatial frequency components. The track profile obtained from both front and rear bogie wheelsets, r_1, r_2 (or s_1, s_2) have the same irregularity but are delayed in the spatial domain by the bogie center distance. However, the sensors are placed on the car body exactly above the front or rear bogie, whichever wheelset is of interest to obtain the precise track profile geometry.

Figs. 3 and 4 are the numerical results obtained using the conventional ASKF method and proposed approach on reconstructing vertical and lateral track profiles for the section from 50 m to 950 m to eliminate the instability due to the filters at the beginning and end of the signal. From the spatial domain responses, as shown in Figs. 3(a) and 4(a), the track profiles are overestimated in the conventional ASKF method, comparing to the proposed approach results, which was significant for the track maintenance. This error

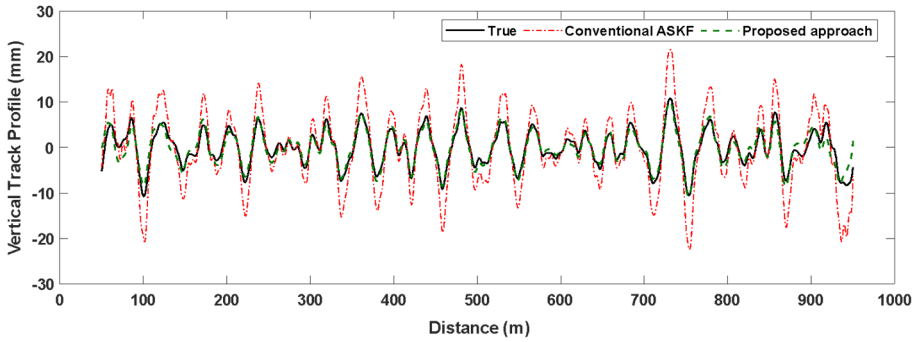

(a) Vertical track profile from 4-DOF train vehicle model

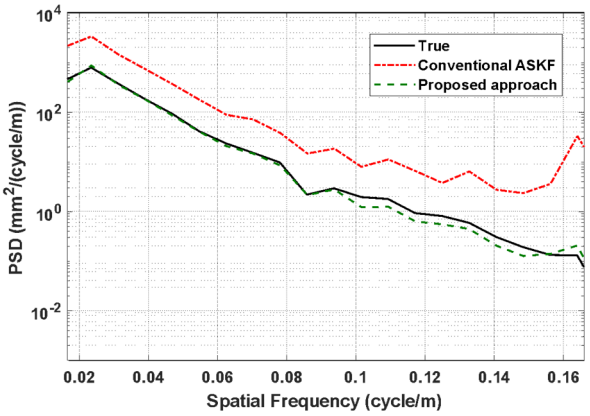

(b) Vertical profile PSD

Fig. 3 Estimation results for vertical track irregularity (section from 50 m to 950 m)

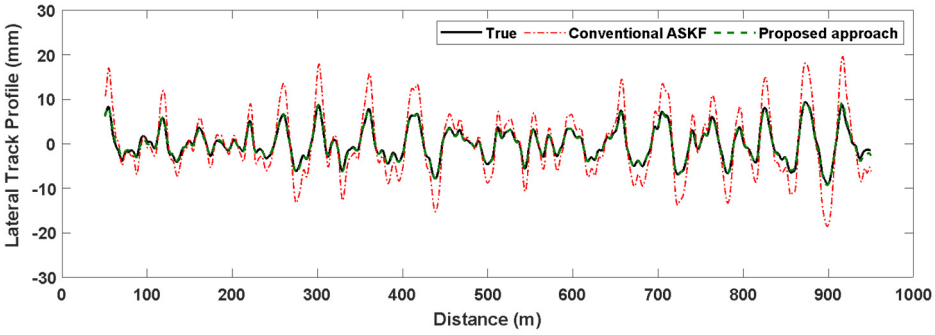

(a) Lateral track profile from 4-DOF train vehicle model

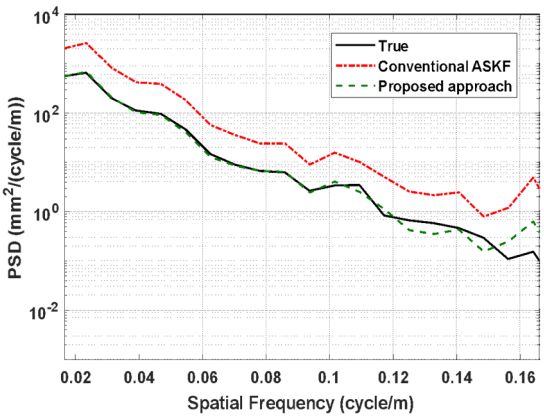

(b) Lateral profile PSD

Fig. 4 Estimation results for lateral track irregularity (section from 50 m to 950 m)

Table 4 Comparison of statistical metrics for vertical and lateral track irregularity (section from 50 to 950 m)

Measurements at train car body	Statistical metrics	Conventional ASKF	Proposed approach
Vertical acceleration and pitching angular velocity	RMSD (%)	109.5	33.38
	CC	0.88	0.94
	RMSE (mm)	4.34	1.32
Lateral acceleration and yawing angular velocity	RMSD (%)	99.37	11.1
	CC	0.93	0.99
	RMSE (mm)	3.65	0.41

is caused due to the observability issues. However, the track profiles estimated through the proposed approach closely match the true profile as the considered train model satisfies the observability condition. PSD plot in Figs. 3(b) and 4(b) show the track irregularities in the spatial frequency domain, which corresponds to the wavelength range from 6 m to 60 m (0.1667 cycle/m to 0.01667 cycle/m). Among the PSD plots, the discrepancy with the frequency component can be observed for the conventional ASKF method.

However, the profile estimated through the proposed approach is in good agreement with the true profile for the wavelength range from 10 m to 60 m (0.1 cycle/m to 0.01667 cycle/m). Also, with a minor difference for the wavelength range of 6 m to 10 m (0.1667 cycle/m to 0.1 cycle/m). The statistical metrics of RMSD, RMSE, and CC are calculated for the section from 50 m to 950 m, as illustrated in Table 4. It is very clear from the metrics that the error is significant for the conventional ASKF method comparing to the proposed approach. Though spatial domain responses look similar for both vertical and lateral profile, from Table 4, the statistical metrics show that the lateral profile result is slightly better than the vertical profile estimation. This may be due to the characteristics of the simulated lateral track profile. Thus, the proposed approach's performance is considered better than the conventional ASKF for both vertical and lateral track profile estimation.

5. Track profile estimation by field test

A field test was performed for collecting responses from an in-service vehicle to validate the proposed approach. The track chosen for the field test was a local railway in Japan, which was about 80 km long with six stations (S). Table 5 illustrates the distance chart between each station for the traversing train vehicle. The existing track conditions were measured using TRV.

A relationship between a true track irregularity and its measured one by 10 m-chord versine method in Japan (Claus and Schiehlen 1998) is mathematically expressed as

$$p(x) = q(x) - \frac{q(x+5) + q(x-5)}{2} \tag{34}$$

where $p(x)$ and $q(x)$ represent the 10 m-chord versine and true track geometry, respectively. In Eq. (34), an independent variable 'x' is the distance measured along the actual track. To validate the profile estimation method, a restored true track profile was converted to 10 m-chord versines. The reference and the estimated profiles were compared in terms of the 10 m-chord versine in the wavelength range from 2.1 m to 14.4 m, which comes under the category of the mid-chord-based measuring system (Grassie 1996).

5.1 On-board monitoring system

A field test was carried out to estimate the track profile using the acceleration and angular velocity obtained from a sensor on the train car body floor. Prevalent sensing devices such as smartphones were potentially utilized for on-board measurement. However, the applicability of such measurement for track profile estimation was not clarified. Apple's iPod touch (Apple Inc. 2018) installed with an iOS application named iDRIMS (2015) was employed. The application was developed with the requirements of precise sampling timing and simple handling operation. iDRIMS can measure acceleration, angular velocity, and GPS signals simultaneously. The vehicle responses were obtained at a sampling frequency of 100 Hz, and the GPS signal was obtained with a sampling frequency of 1 Hz. The sensors were mounted on a plane surface of the train car body floor in the driver room to precisely obtain the measurement data from a vehicle. It was approximately placed above the left front tire of the front bogie along the traversing direction.

The dynamic response data were collected from two types of sensors, as shown in Fig. 5, namely, (a) an On-board rail corrugation monitoring (ORCM) sensor device: developed by Railway Technical Research Institute, Japan (Tanaka *et al*. 2010) and (b) two smartphone devices firmly attached to the top and side surfaces of the black box. On-board rail corrugation monitoring device has been validated in the track maintenance work in Japanese railway

Table 5 Distance chart between stations

Section	1 (S1 - S2)	2 (S2 - S3)	3(S3 – S4)	4 (S4 – S5)	5 (S5 – S6)
Distance (km)	3.53	9	18.1	31.97	17.4

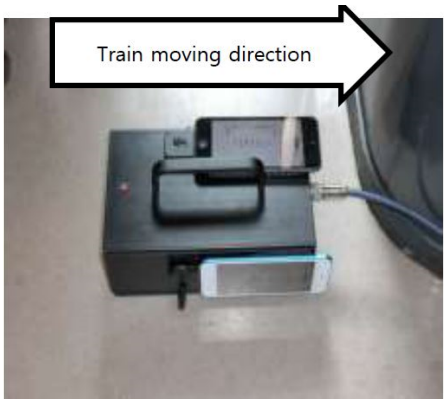

Fig. 5 Sensors placement on train car body floor: smartphones attached to ORCM sensor

companies (Tanaka and Shimizu 2016). The purpose of using multiple sensors on the in-service vehicle was to show the accuracy level among simple sensors and understand the repeatability of the smartphone responses. The two smartphone devices were smartphone-1 (black) and smartphone-2 (blue) in the following sections. The ORCM sensor can only measure acceleration and yawing angular velocity while the smartphone devices can measure acceleration and angular velocity in all three directions. The ORCM sensor was sampled at 5000 Hz, and a low pass filter with a cut-off frequency of 50 Hz was applied. The car body acceleration signals collected by all sensors for an up-train (direction from section 1 to 5) were compared, and only responses for section-3 are shown in Figs. 6(a) and (c) for vertical and lateral direction, respectively. The PSD of the acceleration signals were shown for all sections in Figs. 6(b) and (d) for vertical and lateral direction, respectively.

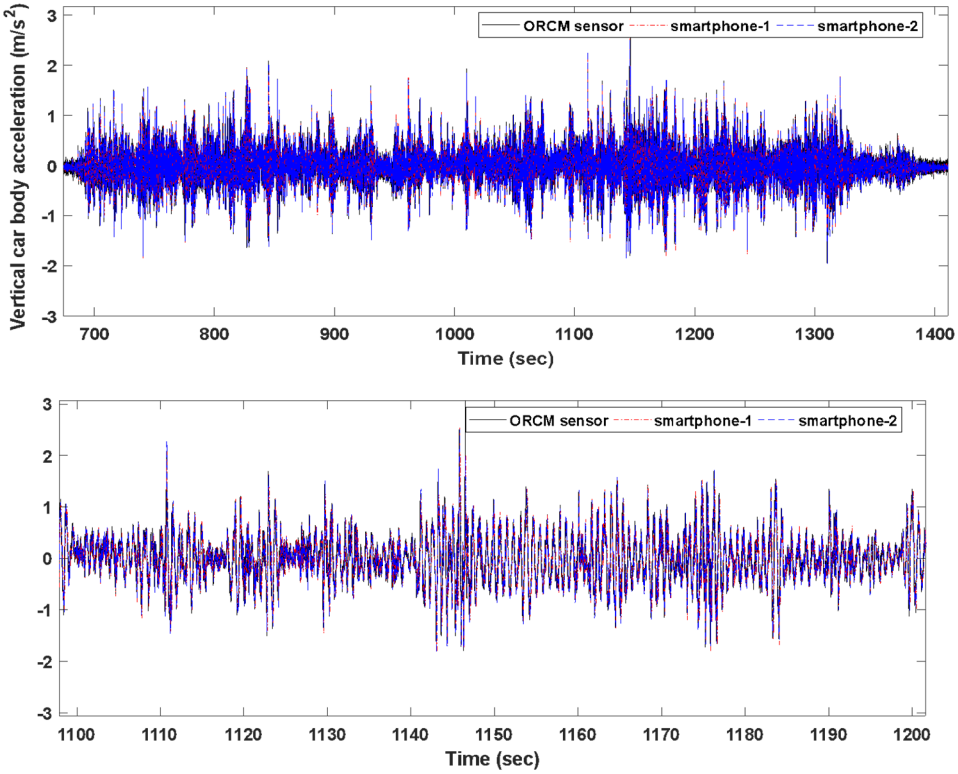

(a) Vertical car body acceleration (section 3 - up train side)

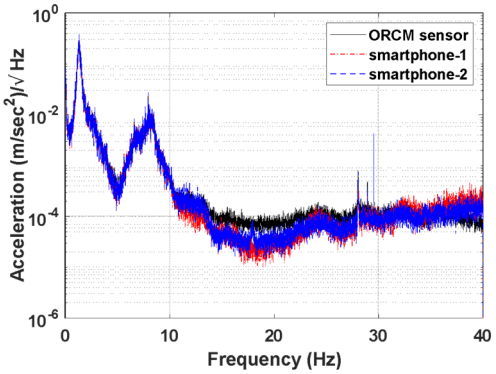

(b) Vertical acceleration PSD (all sections - up train side)

Fig. 6 Comparison of acceleration data among all sensors

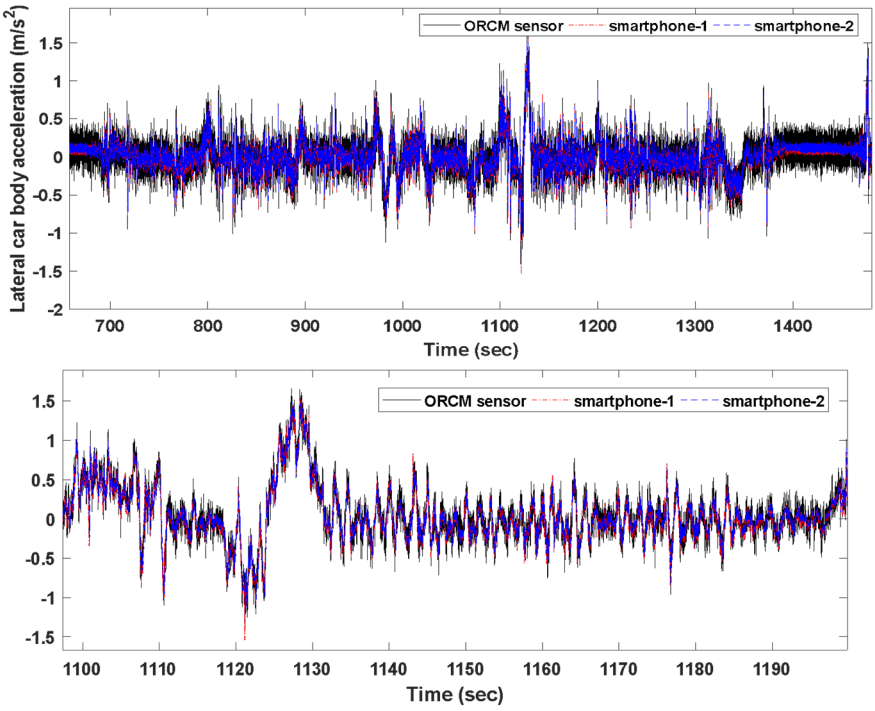

(c) Lateral car body acceleration (section 3 - up train side)

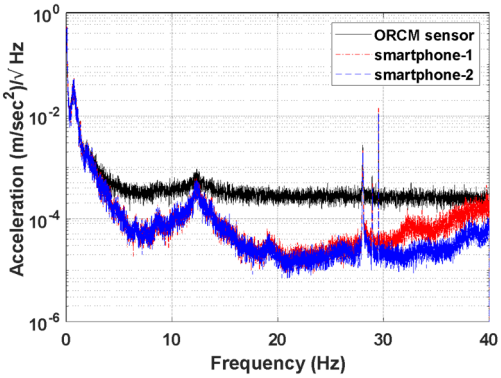

(d) Lateral acceleration PSD (all sections - up train side)

Fig. 6 Comparison of acceleration data among all sensors

From Fig. 6(c), the time history plot of the ORCM sensor shows a high noise level, which is confirmed in the frequency domain plot. Also, the smartphone does not have built-in filters, which can make the signals smoother. The noise level of ORCM sensors was a little higher than the smartphone in the vertical direction. However, the time domain difference was minor, especially for the tremendous response peak value, which was significant for the track maintenance, as shown in the zoomed section of Figs. 6(a) and (c). In lateral acceleration, the smartphone device measurement results showed a satisfaction level of accuracy by comparing with the ORCM sensor, while from the PSD plot (Fig. 6(d)), it is seen that the ORCM sensor had a high noise level. The car body pitching and yawing angular velocity responses measured by two smartphone devices were compared and found to be in good agreement. The velocity profile obtained from the three sensors shows an agreement in Fig. 7. Hence, the accuracy was confirmed for smartphone devices with ORCM sensors for measured vibration responses and running velocity, which can be used in practice. Also, the smartphone devices showed good agreement among themselves. So, in the following sections, only smartphone-2 results are utilized for further analysis.

5.2 Distance sampling method for on-board measured data

The preliminary comparison shows that the track profile obtained from TRV and the estimated profile from in-service vehicle measurement responses do not correlate well since it is not easy to synchronize the different measurement results on the same distance coordinate. The on-board measured data need to be synchronized with TRV results. Tanaka *et al*. (2010) explained a methodology to identify a measurement train vehicle's position by comparing the yawing angular velocity measured on the car body of an in-service train and the transition curve data of the respective track section. It is feasible to match the

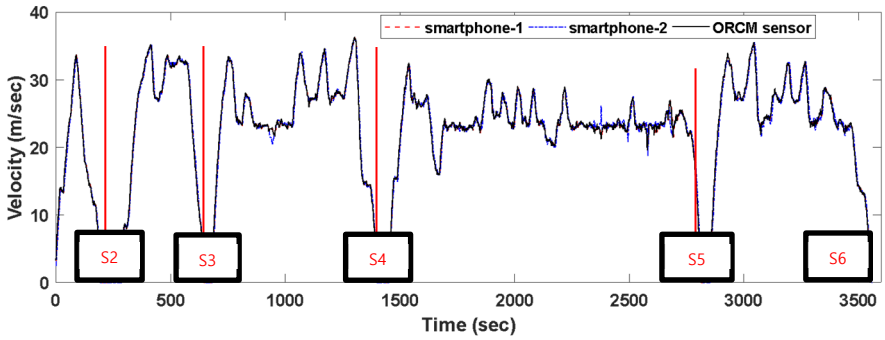

Fig. 7 Comparison of velocity profile among all sensors (up train side)

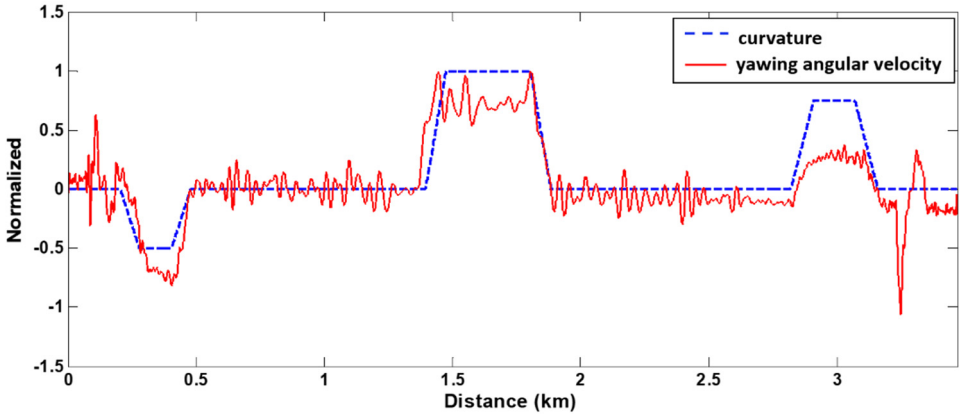

Fig. 8 Comparison of yawing angular velocity and curvature for Section-1

estimated profile and the reference TRV signal by manually correlating the yawing angular velocity and the transition curve data.

Fig. 8 shows the comparison of the yawing angular velocity measured by smartphone-2 and the easement curve (curve radius) of the track section-1 measured using TRV. It can be observed that the matching between curvature and yawing angular velocity is good, especially in the range of 0-2.5 km. After 2.5 km, there is slight deviation for the measured yawing angular velocity. Even though the yaw angular velocity measurement obtained from smartphones have good agreement with the reference OMRC sensors, the responses are influenced by car body vibration characteristics which vary greatly depending on the vehicle type and running speed, and also the track irregularity changes daily. The above-mentioned phenomenon is causing a slight deviation after 2.5 km in the comparison plot of curvature and yaw rate (Fig. 8). The low pass filter with a cut-off frequency of 40 Hz is applied to the smartphone data, and the cross-correlation function is utilized for the comparison. The lag difference is maintained to be zero in all cases. It shows a good correlation among the waveforms, and the distance sampling data is extracted later for the comparison purpose.

5.3 Profile estimation using in-service vehicle responses

The track profiles are estimated using the 4-DOF train model (Fig. 1) and the smartphone-2 sensor data. With this 4-DOF train model, only the axles' average motions on the same bogies are estimated as the input to the train system. The car body vertical acceleration and pitching angular velocity are utilized for estimating vertical profile while car body lateral acceleration and yawing angular velocity are used for estimating lateral profile. The vehicle parameters given in Table 3 are used for the analysis. The velocity profile obtained from smartphone-2 in Fig. 7 is utilized to convert the temporal domain's track profile to the spatial domain. As per the conversion theory proposed by Yoshimura (1995), the estimated track profile is further converted to 10 m-chord versine waveform. Thus, estimated waveforms are comparable to the waveforms obtained from TRV. Fig. 9(a) represents the results for 10 m-chord versines for the vertical profile of the left rail for section 1. The plot compares the track profile obtained from the proposed approach with the reference versine obtained from TRV.

PSD plot in Fig. 9(b) shows the track irregularities in the spatial frequency domain, which corresponds to the wavelength range from 6 m to 60 m (0.1 cycle/m to 0.01667 cycle/m). It also aids to approximately evaluate under which category of irregularity the measured rail track profile section falls. In this case, it matches closely with the FRA - Class 4 (very poor) case. From Fig. 9, the spatial domain plot shows that the basic amplitude levels are close enough for comparison, while the spatial frequency domain plot shows good agreement for wavelength ranging between 10 m to 60 m. The wavelength less than 10 m are not accurate enough to estimate using the proposed algorithm.

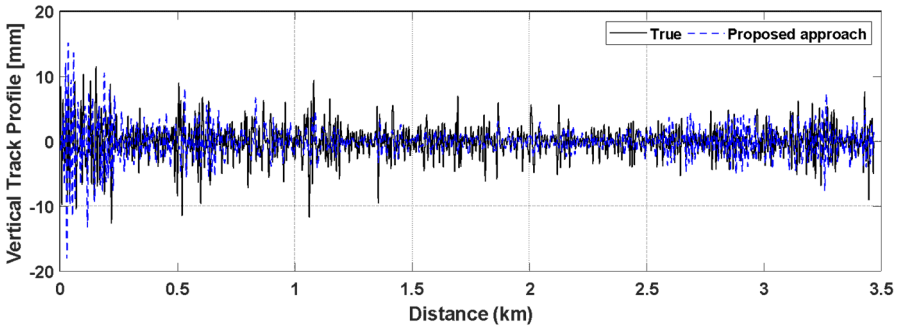

(a) Vertical profile for section 1

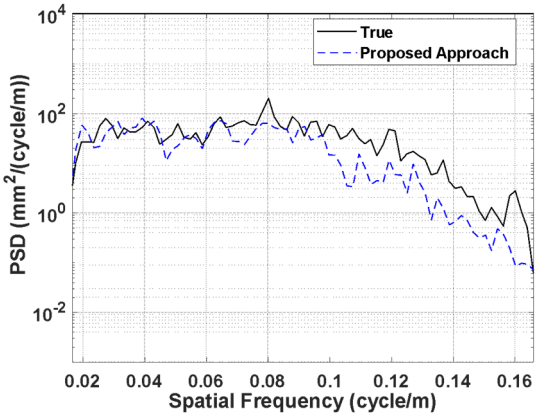

(b) Vertical profile PSD (wavelength of 10 m to 60 m)

Fig. 9 Estimation results for 10 m-chord versines: left vertical profile

There is a slight deviation between 6 m to 10 m, as shown in Fig 9(b). TRV also diagnoses the track in this wavelength range, which is substantial for track maintenance and running safety. The proposed algorithm is further applied to all the remaining sections to estimate the vertical track profile.

Likewise, the 10 m-chord versine results of the left lateral track profile for section 1 are shown in Fig. 10. The plot compares the track profile obtained from the proposed approach with the reference versine obtained from TRV. PSD plot in Fig. 10(b) shows the track irregularities in the spatial frequency domain, which corresponds to the wavelength range from 6 m to 60 m (0.1667 cycle/m to 0.01667 cycle/m). From Fig. 10(a), although the basic amplitude level is closely matching along with the profile, there is a complete mismatch at the distance of 0.8-1.1 km. This is caused because of wheel-rail interaction problem. Besides, from Fig. 10(b), it shows a spike at the range of 0.0285-0.0222 cycle/m. The lateral track profile is mostly affected by hunting oscillation motion and the angle of attack – the tangential angle on the contact point between wheels and rails. The vehicle can make different lateral deflections depending on the angles of the attacks. These are the current limitations that define the train's curving performance, and it predominantly affects lateral force.

The hunting phenomenon, which often occurs when train vehicle runs at high speed and presents a coupled oscillation of the wheelset in its lateral displacement and yaw angle, affects the lateral profile estimation. This kind of motion is caused by wheel conicity and the flange clearance between the wheel and the rail. This phenomenon is complicated to be discussed strictly, but in practice, it could be simplified to be the harmonic oscillation with the wavelength (Tanifuji and Sakuyama 1988) defined by

$$L_h = 2\pi \sqrt{\frac{br}{\lambda}\left[1 + \left(\frac{S_0}{2b}\right)^2\right]} \tag{35}$$

where r is the rolling radius at the center of the wheel tread, $2b$ is the distance between the two contact points of the wheel treads with rails, S_0 is the distance between the two axels of the bogie, λ is the contact angle between the wheel tread and the rail surface. Substituting the data of local in-service train, S_0 = 2.25 m; $2b$ = 1.067 m; $2r$ = 0.81 m; λ = 1/40 into Eq. (35), the wavelength of the hunting motion, L_h, is obtained as 43m. Henceforth, the lateral profile is affected by the hunting motion phenomenon at the wavelength of around 35-45 m (0.0285 – 0.0222 cycle/m), as shown the Fig. 10(b). Similarly, the proposed approach is applied for the other sections to estimate the lateral track profile, and the hunting oscillation phenomenon can be identified for the curved track section.

The statistical metrics like RMSD, CC, and RMSE were utilized to quantify the error among the estimated profile with a true one, as illustrated in Table 6 for vertical and lateral track profile. It is very clear from the statistical metric- CC that the track profile estimated from the proposed approach showed an excellent satisfaction level of accuracy by comparing it with the true profile even though

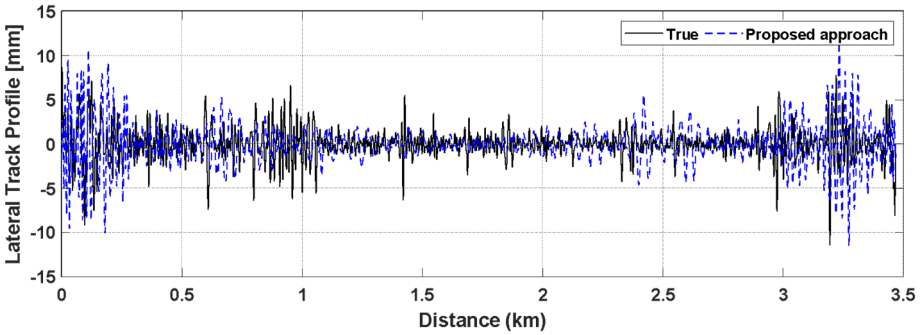

(a) Lateral profile for section 1

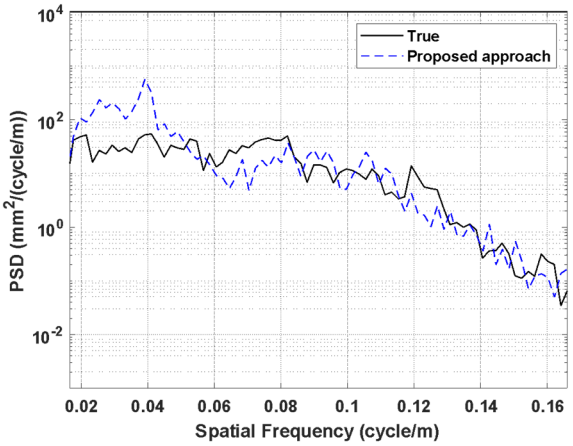

(b) Lateral profile PSD (wavelength of 6 m to 60 m)

Fig. 10 Estimation results for 10 m-chord versines: left lateral profile

Table 6 Comparison of statistical metrics for estimated vertical and lateral profile

Section (Stations)	Vertical profile (10 m – 60 m)			Lateral profile (6 m – 60 m)		
	RMSD (%)	CC	RMSE (mm)	RMSD (%)	CC	RMSE (mm)
1 (S1-S2)	42.3	0.80	1.90	106.3	0.66	2.82
2 (S2-S3)	58.1	0.78	2.68	91.1	0.81	2.36
3 (S3-S4)	86.8	0.79	2.74	89.1	0.62	3.79
4 (S4-S5)	99.8	0.74	3.59	106.4	0.80	3.69
5 (S5-S6)	102.5	0.75	2.89	103.2	0.70	2.84

RMSD error was significant. Also, the RMSE error was minor, which was significant for track maintenance. The possible causes behind the estimation errors in the proposed method are as follows. At first, the proposed observable train model can obtain stable and relatively accurate profile results. However, it was impossible to incorporate some complicated internal or external influence factors in this 4-DOF model, such as the bogie pitching/yawing motion of an actual vehicle, the nonlinearity of the train vehicle suspension systems, and the active control mechanism.

Furthermore, the train's excitation except the track profile has not been considered in the proposed method, such as rail flange contact, gauge deformation, cant, twist in track geometry, and hunting oscillation. These influences need to be further investigated in future research. The real train vehicle primary suspension and secondary suspension systems usually have nonlinearity, especially at high drive speed or considerable track input due to irregularities on the rail. However, this nonlinearity cannot be reproduced by a linear 4 DOF simplified train vehicle model implemented in this study. Another reason is that the train used for the field test is tilting rail cars. The parameter will change during the curve running from the active control mechanism. However, the parameter used is the linear one. Though significant modeling error can be compensated by increasing the system noise covariance, the track profile estimation accuracy may be sacrificed.

6. Discussions

For a practical scenario, the error estimation along the track is much needed rather than the singular value. Therefore, the peak picking and valley picking method is

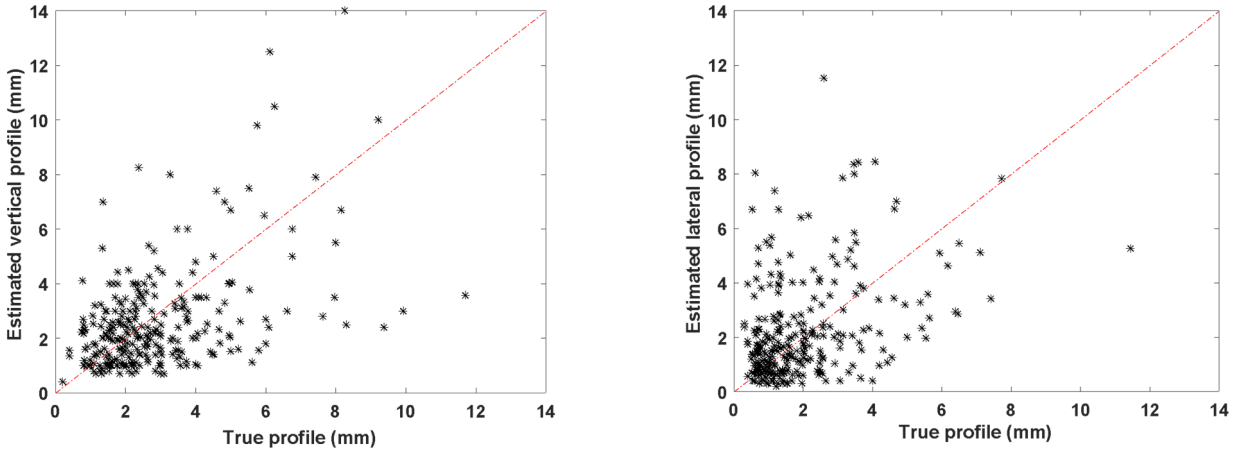

(a) Vertical profile for section 1

(b) Lateral profile for section 1

Fig. 11 Estimation of left vertical and lateral profile in the range of 25 m along the track length

utilized over an average length of 25 m along the track to exclude the higher amplitude values which govern the track irregularity. The average length is 25 m as the length of each is 25 m, and the track irregularity for vertical and lateral profile falls within the range. The true profile entire peak/valley picked values are compared with all the respective values obtained from the estimated profile in Figs. 11(a) and (b) for vertical and lateral track profiles. The estimated 10 m-chord versine waveforms resemble TRV's reference profile with discrepancies, which can be partially explained by hunting oscillation motion for a lateral case. In Fig. 11(a), the distribution of the points is approximately symmetric concerning the bisection of the plot for the vertical profile, while in Fig. 11(b), the points seem to be not symmetrically distributed with respect to the bisection for the lateral profile, with more points present in the upper part of the plot. Subsequently, the part with points for which the estimated lateral profile is higher than the true profile. From the safety point of view, probably having an estimated profile higher than the true profile is probably better than having an estimated profile lower.

The appropriate value for the maintenance threshold can be chosen according to the railway operators' maintenance policy to achieve the desired safety, comfort, and ride quality. The peak picking method will provide fast and precise post-processing track profile error estimation along the track length. It has attempted to identify the optimum maintenance limit for the planning of railway track geometry maintenance. Likewise, the comparison plots can be obtained for all other sections, respectively. Primarily, in a railway vehicle, there is a coupling between the car body's lateral and roll motion and bogies due to the difference in height between the center of mass of these bodies and the line of action of forces generated by the primary and secondary suspensions. Due to this coupling, cross-level irregularities will also excite the bogies and car body's lateral vibration, further to excitation coming from the lateral track profile.

Moreover, the geometry of rails and wheels allows for relative displacement of the two bodies in a lateral direction by an amount of 6-10 mm, comparable to the magnitude of the profile to be estimated (De Rosa *et al*. 2019, 2020). The proposed 4-DOF model is a simplified model, and these coupling effects are not considered in this study. It will be considered and investigated in our future research.

7. Conclusions

The research detailed in this paper has developed a practical inverse analysis scheme for the track profile evaluation by measuring in-service local train vehicle responses. While TRV is often utilized for maintenance purposes, this special vehicle is expensive and difficult to use for small railway operators. Therefore, track profile estimation through in-service vehicle response measurements using smartphones potentially provides efficient and frequent measurement. The appropriate combination and location of sensors and the state-space model of the train have been determined through the observability analysis. The results show that if only the vehicle body motions, i.e., acceleration and angular velocities, are measured, the profile is not observable. Instead of profile at each wheel, the average profile of the same bogie's two wheels is identified using the 4-DOF half car models.

Furthermore, the second derivative of the profile is included as an observable state variable; non-static components of the profile is obtained as the double integration of the state variable. The proposed algorithm is verified through simulations both for the vertical and lateral profile estimation. The 4-DOF model used for the estimation of lateral profile irregularities does not consider the coupling effect between lateral and roll motion of the car body and bogies that occurs due to the difference in height between the center of mass of these bodies and the line of action of forces generated by the primary and secondary suspensions. Due to this coupling, cross-level irregularities will also excite the bogies and car body's lateral vibration, further to excitation coming from the lateral track profile. This coupling effect will be considered and investigated in our future research. The statistical

metrics such as RMSE, RMSD, and CC are utilized for obtaining the error between two waveforms. The peak picking method is utilized for error estimation along the rail track length. The estimated profiles show good agreement with the reference for both the vertical and lateral directions. To validate the proposed estimation algorithm experimentally, track profile estimation using in-service local train vehicle responses measured by smartphone devices is demonstrated. The results are slight deviations due to the simplified 4 DOF model and other phenomena like hunting oscillation motion. This paper proposes and realizes an attempt to use an inverse analysis scheme for the railway track profile estimation from on-board response measurement of local railways. Both numerical analyses and field experiments thus clarify the proposed track profile estimation capability using only one on-board sensing device with the target application of local railway network monitoring, especially for the vital wavelength range for rail maintenance and train running safety. A simplified half-car model cannot represent the bogie pitching/yawing motion of a real train, which is often significant under different conditions. The results are influenced by the wheel-rail flange contact, gauge, cross-level, spiral easement curve, transition gradient, and integration error accumulations. These parameters influence the train dynamics, and thus, measured acceleration and pitch rate at the car body floor is profoundly affected. These influences need to be further investigated. In further research, by utilizing a higher-order train model accounting for bogie pitching/yawing motion, the rail track profile can be estimated more precisely.

Acknowledgments

The first author expresses his sincere appreciation to the Japanese Ministry of Education, Culture, Sports, Science, and Technology (MEXT) for its financial scholarship support during his doctoral study at The University of Tokyo, Japan. This work was supported by JSPS KAKENHI Grant Number JP26630210 and JP19K04570.

References

Apple Inc. (2018), https://www.apple.com

Barke, D. and Chiu, W.K. (2005), "Structural health monitoring in the railway industry: a review", *Struct. Health Monit.*, **4**(1), 81-93. https://doi.org/10.1177/1475921705049764

Bocciolone, M., Caprioli, A., Cigada, A. and Collina, A. (2007), "A measurement system for quick rail inspection and effective track maintenance strategy", *Mech. Sys. Signal Proc.*, **21**(3), 1242-1254. https://doi.org/10.1016/j.ymssp.2006.02.007

Bruni, S., Goodall, R., Mei, T.X. and Tsunashima, H. (2007), "Control and monitoring for railway vehicle dynamics", *Veh. Sys. Dyn.*, **45**(7-8), 743-779. https://doi.org/10.1080/00423110701426690

BS (2003), "Railway applications/Track-Track geometry quality-part 1: characterisation of track geometry", BS EN, 13848-1.

Chatzis, M.N., Chatzi, E.N. and Smyth, A.W. (2015), "On the observability and identifiability of nonlinear structural and mechanical systems", *Struct. Control. Health Monitor.*, **22**(3), 574-593. https://doi.org/10.1002/stc.1690

Chiacchiari, L. and Loprencipe, G. (2015), "Measurement methods and analysis tools for rail irregularities: a case study for urban tram track", *J. Modern Trans.*, **23**(2), 137-147. https://doi.org/10.1007/s40534-015-0070-6

Claus, H. and Schiehlen, W. (1998), "Modeling and simulation of railway bogie structural vibrations", *Veh. Sys. Dyn.*, **29**(S1), 538-552. https://doi.org/10.1080/00423119808969585

De Rosa, A., Alfi, S. and Bruni, S. (2019), "Estimation of lateral and cross alignment in a railway track based on vehicle dynamics measurements", *Mech. Sys. Signal Proc.*, **116**, 606-623. https://doi.org/10.1016/j.ymssp.2018.06.041

De Rosa, A., Kulkarni, R., Qazizadeh, A., Berg, M., Di Gialleonardo, E., Facchinetti, A. and Bruni, S. (2020), "Monitoring of lateral and cross level track geometry irregularities through on-board vehicle dynamics measurements using machine learning classification algorithms", *Proc. Inst. Mech. Eng., Part F: J. Rail. Rapid Transit*, 1-14. https://doi.org/10.1177/0954409720906649

Fauriat, W., Mattrand, C., Gayton, N., Beakou, A. and Cembrzynski, T. (2016), "Estimation of road profile variability from measured vehicle responses", *Veh. Sys. Dyn.*, **54**(5), 585-605. https://doi.org/10.1080/00423114.2016.1145243

Fries, R.H. and Coffey, B.M. (1990), "A state-space approach to the synthesis of random vertical and crosslevel rail irregularities", *J. Dyn. Sys. Meas. Control.*, **112**(1), 83-87. https://doi.org/10.1115/1.2894143

Giurgiutiu, V. and Rogers, C.A. (1998). "Recent advancements in the electromechanical (E/M) impedance method for structural health monitoring and NDE", *Proceedings of SPIE 3329, Smart Structures and Materials 1998: Smart Structures and Integrated Systems*, 3329, San Diego, CA, USA, July, pp. 536-547. https://doi.org/10.1117/12.316923

Grassie, S.L. (1996), "Measurement of railhead longitudinal profiles: a comparison of different techniques", *Wear*, **191**(1-2), 245-251. https://doi.org/10.1016/0043-1648(95)06732-9

Hermann, R. and Krener, A. (1977), "Nonlinear controllability and observability", *IEEE Trans. Auto. Control*, **22**(5), 728-740. https://doi.org/10.1109/TAC.1977.1101601

iDRIMS measurement (2015), Dynamic Response Intelligent Monitoring System measurement app for, iOS.

Ishii, H., Fujino, Y., Mizuno, Y. and Kaito, K. (2006), "The Study of Train Intelligent Monitoring System using acceleration of ordinary trains", *Proceedings of Asia-Pacific Workshop on Structural Health Monitoring*, Yokohama, Japan, December.

JRCEA (2002), Investigation committee of railway technical specification in civil engineering, ed. J.R.C.E. Association, Japan: Ministry of Land, Infrastructure, Transport and Tourism: Railway technical specification (civil engineering). [In Japanese]

JSME (1996), Dynamics of Rolling Stock, ed. J.S.o.M. Engineers, Denkisya-Kenkyukai. [In Japanese]

Kalman, R.E. (1963), "Mathematical description of linear dynamical systems", *J. Soc. Industrial App. Math., Series A: Control*, **1**(2), 152-192. https://doi.org/10.1137/0301010

Kobayashi, T., Naganuma, Y. and Tsunashima, H. (2014), "Condition Monitoring of Shinkansen Tracks based on Inverse Analysis", *Int. J. Performability Eng.*, **10**(5), 443-452. https://doi.org/10.23940/ijpe.14.5.p443.mag

Kojima, T., Tsunashima, H. and Matsumoto, A. (2006), "Fault detection of railway track by multi-resolution analysis", *Computers in Railways X*, 88, 955-964, WIT Transactions on The Built Environment, WIT Press, Southampton, UK. https://doi.org/10.2495/CR060931

Lourens, E., Reynders, E., De Roeck, G., Degrande, G. and Lombaert, G. (2012), "An augmented Kalman filter for force identification in structural dynamics", *Mech. Sys. Signal Proc.*, **27**, 446-460. https://doi.org/10.1016/j.ymssp.2011.09.025

Naganuma, Y. and Sato, Y. (2000), "Track state control with use of real time digital data processing", *Int. J. Heavy Vehicle Syst.*, **7**(1), 82-95. https://doi.org/10.1504/IJHVS.2000.004451

OBrien, E.J., Bowe, C., Quirke, P. and Cantero, D. (2017), "Determination of longitudinal profile of railway track using vehicle-based inertial readings", *Proc. Inst. Mech. Eng., Part F: J. Rail. Rapid Transit*, **231**(5), 518-534. https://doi.org/10.1177/0954409716664936

OBrien, E.J., Quirke, P., Bowe, C. and Cantero, D. (2018), "Determination of railway track longitudinal profile using measured inertial response of an in-service railway vehicle", *Struct. Health Monitor.*, **17**(6), 1425-1440. https://doi.org/10.1177/1475921717744479

Odashima, M., Azami, S., Naganuma, Y., Mori, H. and Tsunashima, H. (2017), "Track geometry estimation of a conventional railway from car-body acceleration measurement", *Mech. Eng. J.*, **4**(1), 16-00498. https://doi.org/10.1299/mej.16-00498

Park, G. and Inman, D.J. (2007), "Structural health monitoring using piezoelectric impedance measurements", *Phil. Trans. Royal Soc. A: Math., Phy. Eng. Sci.*, **365**(1851), 373-392. https://doi.org/10.1098/rsta.2006.1934

Real, J., Salvador, P., Montalbán, L. and Bueno, M. (2011), "Determination of rail vertical profile through inertial methods", *Proc. Inst. Mech. Eng., Part F: J. Rail. Rapid Transit*, **225**(1), 14-23. https://doi.org/10.1243/09544097JRRT353

Saravanan, T.J., Zhao, B., Su, D. and Nagayama, T. (2016), "An observability analysis for profile estimation through vehicle response measurement", *Transforming the Future of Infrastructure through Smarter Information: Proceedings of the International Conference on Smart Infrastructure and Construction*, ICE Publishing, Cambridge, UK, June, pp. 357-362.

Su, D., Fujino, Y., Nagayama, T., Hernandez Jr, J.Y. and Seki, M. (2010), "Vibration of reinforced concrete viaducts under high-speed train passage: measurement and prediction including train–viaduct interaction", *Struct. Infra. Eng.*, **6**(5), 621-633. https://doi.org/10.1080/15732470903068888

Sunaga, Y., Sano, I. and Ide, T. (1997), "A method to control the short wave track irregularities utilizing axle box acceleration", *Railway Tech. Research Inst., Quart. Reports*, **38**(4), 176-181.

Tanaka, H. and Shimizu, A. (2016), "Practical application of portable trolley for the continuous measurement of rail surface roughness for rail corrugation maintenance", *Quarterly Report of RTRI*, **57**(2), 118-124. https://doi.org/10.2219/rtriqr.57.2_118

Tanaka, H., Saruki, Y. and Haga, A. (2010), "Distance sampling method of on-board measured data for portable track condition monitoring device", *Proceedings of the 17th Railway Technology Union Symposium*, Japan.

Tanaka, H., Matsumoto, M., Miwa, M. and Miyazaki, Y. (2017), "Comparison analysis of various evaluation indexes of track irregularity data for high-speed railway track", *Proceedings of Railway Engineering 2017*, Edinburgh, UK, June.

Tanifuji, K. and Sakuyama, T. (1988), "The Characteristics of Wheel Wear in Shinkansen Electric Cars and Its Effect on the Running Vibration: In Case of Conical-Shaped Wheels with a Conicity of 1/40", *JSME Int. J. Ser. 3, Vib., Ctrl. Eng., Eng. for Industry*, **31**(2), 457-464. https://doi.org/10.1299/jsmec1988.31.457

Tsunashima, H., Naganuma, Y. and Kobayashi, T. (2014), "Track geometry estimation from car-body vibration", *Veh. Sys. Dyn.*, **52**(sup1), 207-219. https://doi.org/10.1080/00423114.2014.889836

Ward, C.P., Weston, P.F., Stewart, E.J.C., Li, H., Goodall, R.M., Roberts, C., Mei, T.X., Charles, G. and Dixon, R. (2011), "Condition monitoring opportunities using vehicle-based sensors", *Proc. Inst. Mech. Eng., Part F: J. Rail. Rapid Transit*, **225**(2), 202-218. https://doi.org/10.1177/09544097JRRT406

Weston, P.F., Ling, C.S., Roberts, C., Goodman, C.J., Li, P. and Goodall, R.M. (2007a), "Monitoring vertical track irregularity from in-service railway vehicles", *Proc. Inst. Mech. Eng., Part F: J. Rail. Rapid Transit*, **221**(1), 75-88. https://doi.org/10.1243/0954409JRRT65

Weston, P.F., Ling, C.S., Goodman, C.J., Roberts, C., Li, P. and Goodall, R.M. (2007b), "Monitoring lateral track irregularity from in-service railway vehicles", *Proc. Inst. Mech. Eng., Part F: J. Rail. Rapid Transit*, **221**(1), 89-100. https://doi.org/10.1243/0954409JRRT64

Weston, P., Roberts, C., Yeo, G. and Stewart, E. (2015), "Perspectives on railway track geometry condition monitoring from in-service railway vehicles", *Veh. Sys. Dyn.*, **53**(7), 1063-1091. https://doi.org/10.1080/00423114.2015.1034730

Xue, K., Nagayama, T. and Zhao, B. (2020), "Road profile estimation and half-car model identification through the automated processing of smartphone data", *Mech. Sys. Signal Proc.*, 142, 106722. https://doi.org/10.1016/j.ymssp.2020.106722

Yoshimura, A. (1995), "Theory and practice for restoring an original waveform of a railway track irregularity", *Railway Tech. Research Inst., Quart. Reports*, **36**(2), 85-94.

Zhao, B., Nagayama, T. and Xue, K. (2019), "Road profile estimation, and its numerical and experimental validation, by smartphone measurement of the dynamic responses of an ordinary vehicle", *J. Sound Vib.*, **457**, 92-117. https://doi.org/10.1016/j.jsv.2019.05.015

Appendices

Appendix A: *For vertical displacement*

The dynamic equation of motion for the 4-DOF vertical model (Fig. 1(a)) is given in Eq. (1), and it is derived using the following matrices

$$\mathrm{M}_v = \begin{bmatrix} m_c & 0 & 0 & 0 \\ 0 & I_c & 0 & 0 \\ 0 & 0 & m_{t1} & 0 \\ 0 & 0 & 0 & m_{t2} \end{bmatrix} \tag{A1}$$

$$C_v = \begin{bmatrix} 2c_s & 0 & -c_s & -c_s \\ 0 & 2c_s l_c^2 & -l_c c_s & l_c c_s \\ -c_s & -l_c c_s & 2c_p + c_s & 0 \\ -c_s & l_c c_s & 0 & 2c_p + c_s \end{bmatrix} \tag{A2}$$

$$K_v = \begin{bmatrix} 2k_s & 0 & -k_s & -k_s \\ 0 & 2k_s l_c^2 & -l_c k_s & l_c k_s \\ -k_s & -l_c k_s & 2k_p + k_s & 0 \\ -k_s & l_c k_s & 0 & 2k_p + k_s \end{bmatrix} \tag{A3}$$

$$D = \begin{bmatrix} 0 & 0 \\ 0 & 0 \\ 2k_p & 0 \\ 0 & 2k_p \end{bmatrix} \qquad E = \begin{bmatrix} 0 & 0 \\ 0 & 0 \\ 2c_p & 0 \\ 0 & 2c_p \end{bmatrix} \tag{A4}$$

$$A_a = \begin{bmatrix} 0_{4x4} & I_{4x4} & 0_{6x4} \\ -M_v^{-1}K_{v(4x4)} & -M_v^{-1}C_{v(4x4)} & a^*_{2x4} \\ 0_{4x4} & 0_{4x6} & \begin{matrix} I_{2x2} \\ 0_{2x2} \end{matrix} \end{bmatrix} \tag{A5}$$

$$a^* = \begin{bmatrix} \frac{2k_p}{m_{t1}} & 0 & \frac{2c_p}{m_{t1}} & 0 & 0 & \frac{2k_p}{m_{t2}} & 0 & \frac{2c_p}{m_{t2}} \end{bmatrix}$$

where, m_c is the mass for the vehicle car body; I_c is the mass moment of inertia for the vehicle car body; m_{t1} and m_{t2} are the masses of the front/rear bogies respectively; c_p and c_s are the vertical damping coefficients of primary and secondary suspensions respectively; k_p and k_s are the vertical spring stiffness of primary and secondary suspensions respectively; $2l_c$ and $2l_t$ are car body base and bogie-wheel base, respectively; A_a is the transition matrix of the augmented state vector corresponding to conventional ASKF.

Appendix B: *For lateral displacement*

The dynamic equation of motion for the 4-DOF lateral model (Fig. 1(b)) is given in Eq. (2). The mass matrix $[M_l]$ is identical in form to $[M_v]$ given in Eq. (A1). The damping matrix $[C_l]$ is given as

$$C_l = \begin{bmatrix} 2c_{sh} & 0 & -c_{sh} & -c_{sh} \\ 0 & 2c_{sh} l_b^2 & -l_b c_{sh} & l_b c_{sh} \\ -c_{sh} & -l_b c_{sh} & 2c_{ph} + c_{sh} & 0 \\ -c_{sh} & l_b c_{sh} & 0 & 2c_{ph} + c_{sh} \end{bmatrix} \tag{B1}$$

The stiffness matrix $[K_l]$ is identical in form to $[C_l]$ given in Eq. (B1) except that the related term 'c' should be replaced by 'k'. The transition matrix A_a of the system in the state-space representation is similar to Eq. (A5) except that the corresponding term $[M_v]$ $[K_v]$ and $[C_v]$ should be replaced by $[M_l]$ $[K_l]$ and $[C_l]$ respectively. The notations, c_{ph} and c_{sh} are the horizontal damping coefficients of primary and secondary suspensions respectively; k_{ph} and k_{sh} are the horizontal spring stiffness of primary and secondary suspensions respectively; $2l_b$ and $2l_r$ are car body base and bogie-wheel base, respectively.

Appendix C: *Transition matrix corresponding to proposed ASKF*

The transition matrix of the augmented state vector corresponding to the proposed ASKF method as per Eq. (24) is expressed as

$$A_a = \begin{bmatrix} 0_{4x4} & I_{4x4} & 0_{6x6} \\ -M_v^{-1}K_{v(4x4)} & -M_v^{-1}C_{v(4x4)} & a^*_{2x6} \\ 0_{6x8} & \begin{matrix} I_{4x4} \\ 0_{2x4} \end{matrix} & 0_{6x2} \end{bmatrix} \tag{C1}$$

$$a^* = \begin{bmatrix} \frac{2k_p}{m_{t1}} & 0 & \frac{2c_p}{m_{t1}} & 0 & 0 & 0 & \frac{2k_p}{m_{t2}} & 0 & \frac{2c_p}{m_{t2}} & 0 & 0 \end{bmatrix}$$